Physics-Informed Neural ODE with Heterogeneous Control Inputs (PINOHI) for Quality Prediction of Composite Adhesive Joints

Yifeng Wang[a,b], Shancong Mou[c], Jianjun Shi[a,b] and Chuck Zhang[a,b]*

[a]H. Milton Stewart School of Industrial and Systems Engineering, Georgia Institute of Technology, Atlanta, GA, USA; [b]Georgia Tech Manufacturing Institute, Georgia Institute of Technology, Atlanta, GA, USA; [c]Department of Industrial and Systems Engineering, University of Minnesota, Twin Cities, Minneapolis, MN, USA

Abstract

Composite materials have long been used in various industries due to their superior properties such as high strength, lightweight and corrosive resistance. Bonded composite joints are finding increasing applications as they provide extensive structural benefits and design flexibility. On the other hand, the failure mechanism of composite adhesive joints is not fully understood. A model that bridges manufacturing parameters and final quality measures is highly desired for the design and optimization of the composite adhesive joints manufacturing process. In this study, a novel framework of physics-informed Neural Ordinary Differential Equation (ODE) with heterogeneous control input (PINOHI) is proposed, which links the heterogeneous manufacturing parameters to the final bonding quality of composite joints. The proposed model structure is heavily motivated by engineering knowledge, by incorporating a calibrated mathematical physics model into the Neural ODE framework, which can significantly reduce the number of data samples required from costly experiments while maintaining high prediction accuracy. The proposed PINOHI model is implemented in the quality prediction of composite adhesive joints bonding problem. A set of experiments and associated data analytics are conducted to demonstrate the superior property of the PINOHI model by using both the leave-one-batch-out cross-validation and sensitivity analysis.

Keywords: Composite, joining, Neural ODE, physics-informed machine learning

1. Introduction

With the increasing use of composite materials in aviation and aerospace industries for weight reduction and energy efficiency improvement, adhesive joining gains much more interest at an unprecedented rate as a major manufacturing process. Composite adhesive joining uses specially designed adhesive pastes or films to bond composite panels. Compared to traditional mechanical fasteners, such as riveted or bolted joints, composite adhesive joining can significantly reduce weight and avoid material damage and stress concentrations.

As shown in Figure 1 and Table 1, composite adhesive joints are made from complicated, multi-stage manufacturing processes (MMP), involving material thawing, panel fabrication, surface treatment, and joints curing, followed by a lap shear testing process. The input (control variables) and output for each stage of the MMP can be multiple heterogeneous manufacturing parameters, in the form of scalar, functional curve, matrix, and tensor, whose effects can propagate from the current stage to the downstream stages and finally impact the bonding quality. In addition, the anisotropy of composite materials and the chemical and physical reactions during each stage also add to the complexity.

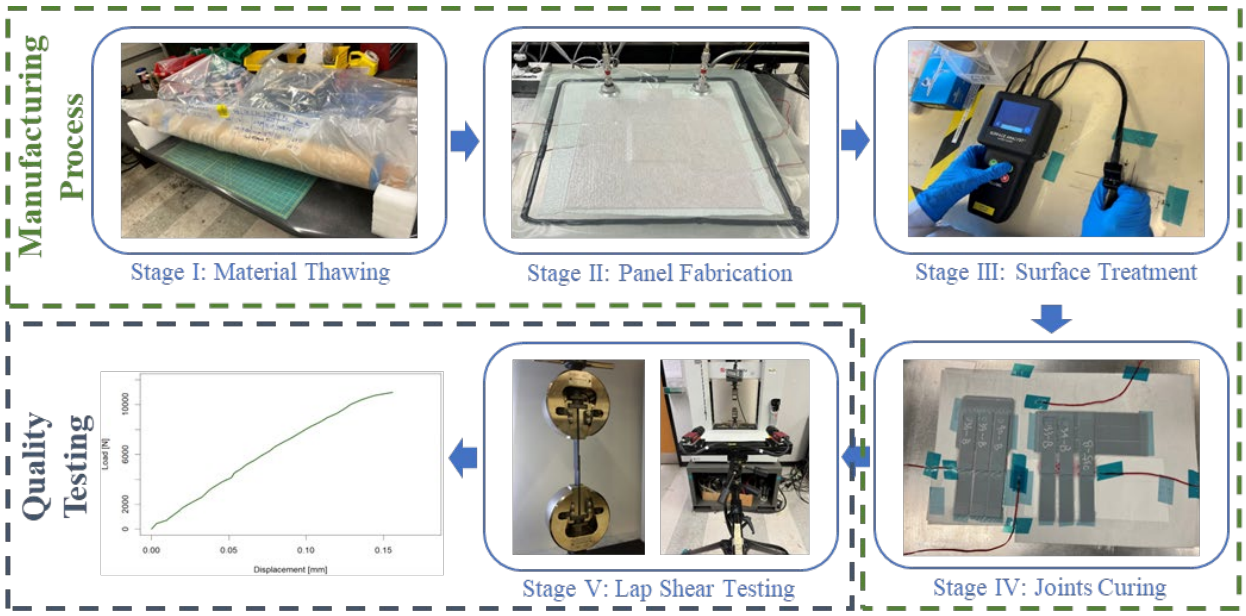

Fig. 1: Multistage manufacturing processes of composite adhesive joints.

Accurate mechanical property understanding and characterization of the adhesive bonded joints, with respect to the manufacturing process, is not only of critical safety consideration but also important in bonding quality prediction, design optimization, and root cause diagnosis. A common metric of the bonding quality is the bonding strength which is the output of a destructive test of lap joints. Such mechanical tests generate load-displacement curves that characterize the mechanical property of the adhesive bonding. Based on the load-displacement curves, one can further derive stress-strain curves, bonding strength, overall bonding stiffness at different strain levels, total energy required to cause failure, etc. However, destructive tests are often expensive and time-consuming.

Table 1: Heterogeneous manufacturing parameters involved in MMP of composite adhesive joints.

Stage	Heterogeneous Manufacturing Parameters					
	Input		Output		Environ. Factor	
	Var.	Description	Var.	Description	Var.	Description
I	N/A	N/A	$t_{out}^{C} \in \mathbb{R}$	Total out-of-freezer time of adherend [s]	N/A	N/A
	N/A	N/A	$t_{out}^{A} \in \mathbb{R}$	Total out-of-freezer time of adhesive [s]	N/A	N/A
II	$r^F \in \mathbb{R}$	Ramp-up rate [°C/s]	$\boldsymbol{T}^F(t) \in \mathbb{R}^{t^F \times 2 \times 2}$	TC readings [°C]	$T_e^F \in \mathbb{R}$	Ambient temp. [°C]
	$t^F \in \mathbb{R}$	Dwelling time [s]	$\boldsymbol{T}_{avg}^F \in \mathbb{R}^{2\times 2}$	Avg. TC reading [°C]	$H_e^F \in \mathbb{R}$	Relative humidity [%]
	$T^F \in \mathbb{R}$	Dwelling temp. [°C]	$\boldsymbol{p}^F(t) \in \mathbb{R}^{t^F}$	Vac. reading [Pa]	N/A	N/A
	$p^F \in \mathbb{R}$	Vac. pressure [Pa]	$p_{min}^F \in \mathbb{R}$	Min. pressure [Pa]	N/A	N/A
	$g \in \mathbb{R}$	Sandpaper grit [-]	$b, c, t, l, t_a \in \mathbb{R}$	Geometric dim. [mm]	N/A	N/A
III	$X_C \in \{0,1\}$	Categ. var. of contamination [-]	$\boldsymbol{\Psi}_A, \boldsymbol{\Psi}_B \in \mathbb{R}^{2\times 2}$	Contact angle dist. of panel A, B [°]	N/A	N/A
IV	$r^J \in \mathbb{R}$	Ramp-up rate [°C/s]	$\boldsymbol{T}^J(t) \in \mathbb{R}^{t^J \times 2 \times 2}$	TC readings [°C]	$T_e^J \in \mathbb{R}$	Ambient temp. [°C]
	$t^J \in \mathbb{R}$	Dwelling time [s]	$\boldsymbol{T}_{avg}^J \in \mathbb{R}^{2\times 2}$	Avg. TC reading [°C]	$H_e^J \in \mathbb{R}$	Relative humidity [%]
	$T^J \in \mathbb{R}$	Dwelling temp. [°C]	$\boldsymbol{p}^J(t) \in \mathbb{R}^{t^J}$	Vac. reading [Pa]	N/A	N/A
	$p^J \in \mathbb{R}$	Vac. pressure [Pa]	$p_{min}^J \in \mathbb{R}$	Min. pressure [Pa]	N/A	N/A
	N/A	N/A	$X_F \in \{0,1,2\}$	Categ. var. of flash [-]	N/A	N/A
V	$s \in \mathbb{R}$	Load rate [mm/s]	$\boldsymbol{F}(\delta) \in \mathbb{R}^{\delta_{tot}}$	Load-disp. curve [N]	N/A	N/A

In order to proceed to the downstream tasks such as design optimization and root cause diagnosis, it is highly desirable to develop an end-to-end model that links heterogeneous manufacturing parameters in the manufacturing processes and the output of the destructive testing process for bonding quality prediction. Numerous efforts on physics-based modeling (Deb et al., 2008; Owens and Lee-Sullivan, 2000a; Zimmermann et al., 2022) have been made to understand the lap shear testing process. In those studies, assumptions are typically made that the lap shear testing process is governed by a set of ordinary/partial differential equations (ODEs/PDEs). Computer simulations, such as finite element analysis (FEA), are utilized to emulate the underlying relationships. However, such simulations are often computationally expensive and suffer from over-simplified assumptions. Also, those models often take material properties (e.g., Young's modulus, Poisson's ratio) and geometric dimensions as inputs, and the bonding strength or

stiffness as the output/result. These material properties are results of the upstream manufacturing stages, which are often unknown functions of the manufacturing parameters and cannot be measured directly. Additionally, due to the complex chemical and physical interactions and heterogeneous process parameters during manufacturing processes, physics-based models usually restrain their scopes to the mechanical testing stage itself.

On the other hand, researchers also explored data-driven models (Kang et al., 2021; Wang et al., 2023), attempting to bridge manufacturing parameters and mechanical properties. This usually requires massive amounts of experimental data to build a model with high confidence, especially when there are multiple heterogeneous process parameters involved. Such methods are typically infeasible for composite adhesive joints because costly destructive tests lead to data scarcity in practice.

To mitigate the issue of lacking labeled data for training, combining physics-based models and data-driven methods to exploit the advantages of each technique is of significance. The lap shear testing stage shown in Fig. 1 can be estimated as a collection of springs (Owens and Lee-Sullivan, 2000a) under a quasi-static tensile loading with certain assumptions, which is a first-order dynamical ODE system in terms of load with respect to displacement. With unknown system parameters determined by the manufacturing parameters, the Neural ODE (Chen et al., 2018) will be a natural choice to model this system. However, the original Neural ODE structure only takes the system state with its derivatives as inputs, ignoring related manufacturing parameters in the upstream stages. In other words, it focuses on the evolution of the system state in the testing stage, but not the relationships between those manufacturing parameters with the quality measures of the final product. Besides, Neural ODE incorporates physics by approximating the underlying ODE using a neural network instead of considering any known or partially known governing physical equations.

To address these challenges of data shortage and end-to-end physics learning, a novel framework of the Neural ODE structure with additional heterogeneous manufacturing control inputs and explicit physical knowledge embedding (PINOHI) is proposed. It addresses those challenges and difficulties by

1. Integrating *physics knowledge* into the Neural ODE framework in addition to the ODE structure.
2. Generalizing the Neural ODE framework by incorporating additional upstream *heterogeneous* manufacturing parameters as control inputs, such that it can leverage product quality and process features and be used for control purposes.
3. Pre-determining the model structure for variable selection based on *engineering domain knowledge* to reduce the amount of training data required for obtaining adequate accuracy.
4. Optimizing the data-driven model and the calibration process of the physics-based model in an *end-to-end* fashion to obtain a better predictive performance.

The primary contribution of this article lies in the application of a novel modeling framework to the field of composite material/structure manufacturing and maintenance, which involve complicated processes yet lacking adequate physical understanding. Unlike existing efforts focusing only on the testing process (stage V in Fig. 1) modeling of composite adhesive joints, the proposed PINOHI framework is an end-to-end model that takes heterogeneous manufacturing parameters as inputs and covers both manufacturing and testing processes (stages I-V in Fig. 1), which provides a key contribution and insight to quality characterization and downstream manufacturing optimization. Specifically, the contributions of this article are summarized as follows:

1. We propose a novel modeling framework, PINOHI, for quality prediction using heterogeneous manufacturing parameters, which is the first end-to-end model for the application of composite adhesive joints. It is a pioneering framework of the Neural ODE structure with additional heterogeneous manufacturing control inputs and explicit physical knowledge embedding.
2. The proposed PINOHI framework integrates the known/partially known physics knowledge and the modeling capability of the Neural ODE structure in solving dynamical systems, achieving superior predictive performance with limited experiment data.

3. The proposed PINOHI framework is extendable to general dynamical systems where the governing equation is an ODE given physics knowledge that can be represented by an analytical model or numerical method.

The remainder of this article is organized as follows. Section 2 gives a brief literature review of related work. Then, the proposed PINOHI framework is introduced in Section 3. In Section 4, the application of the proposed framework to quality prediction of composite adhesive joints is presented. Finally, a conclusion and outline of future research directions are discussed in Section 5.

2. Related Work

The composite in this paper specifically refers to carbon fiber reinforced polymer (CFRP). The adhesive joint configuration is the classic single-lap joint, whose modeling has been extensively studied (Banea and da Silva, 2009). The majority of existing modeling work focuses on physics-based methods. The typical physics-based model for the testing processes of brittle composite adhesive joints is the cohesive zone model (CZM) (Dugdale, 1960) with a simplified bi-linear (triangular) traction-separation law and a homogeneity assumption in FEA to emulate the evolution of fracture process. Early attempts (Pereira et al., 2010; Song et al., 2010) were made to explore the relationship between manufacturing parameters (or methods) and the bonding quality through an experimental or numerical way. Utilizing CZM, a parametric numerical study was conducted by Neto et al. (2012) on single-lap joints with different adhesives and overlap lengths to predict bonding strength. Campilho et al. (2013) compared different CZM laws with triangular, exponential, and trapezoidal shapes for single-lap joints with brittle and ductile adhesives where the numerical results agree with experimental data well in the linear stage but not for the following nonlinearity in the load-displacement curve. Nastos and Zarouchas (2022) developed a stochastic finite element model considering the uncertainties of mechanical properties of the constituent materials, focusing on strength prediction.

In addition to finite element simulations, mechanics-based theoretical results were also explored by researchers. Owens and Lee-Sullivan (2000a, 2000b) developed a theoretical model for the stiffness behaviour in the adhesively bonded composite-to-aluminium single-lap joint. They modeled it as a collection of springs which is a first-order dynamical system and verified it through an experimental study, which generally predicts well for the stiffness change due to crack growth. Considering out-of-plane deflection due to tensile loading and asymmetric geometry, Zimmermann et al. (2022) derived an analytical estimate of the adhesive bonding stiffness, which offers a more comprehensive result.

Physics-based models often rely on strong assumptions about material and geometric properties which will lead to model discrepancy. In addition, they can only model the testing process, whose inputs are usually unknown functions of manufacturing parameters. Therefore, additional modeling effort is needed to further (i) calibrate the physical model; and (ii) bridge the end-to-end relationship between manufacturing parameters and final quality measure. For the first point, data-driven methods are used. Gu et al. (2021) predicted the failure load of joints using a deep neural network (DNN) with geometric and material inputs to obtain the optimal design of the structure. Freed et al. (2022) utilized Gaussian Process Regression (GPR) to find the optimal failure parameters trained by mixed mode bending samples simulated by CZM. These parameters were then verified by resultant failure strength with different adhesive thicknesses. While for models that attempt to link manufacturing parameters with final quality measures, they are not fully explored. Preliminary efforts (Kang et al., 2021; Sommer et al., 2022; Wang et al., 2023) were made to reveal the connection between the manufacturing parameters and mechanical properties of the adhesive itself using machine learning methods, rather than the whole manufacturing process. Rangaswamy et al. (2020) linked two manufacturing parameters, bonding length and adhesive thickness, to the bonding strength using a DNN, which are only a small subset of all manufacturing parameters.

Physics-informed machine learning (PIML) has great potential to simultaneously complete the two tasks, physical model calibration and end-to-end modeling, by seamlessly incorporating known or partially known mathematical physics models with data (Karniadakis et al., 2021). Adopting a physics-informed loss function to incorporate the governing PDE, Raissi et al. (2019) proposed a physics-informed neural network

(PINN) framework for forward and inverse problems. Z. Chen et al. (2021) integrated sparse regression with PINN to efficiently identify the key parameters from scarce data for PDE discovery from nonlinear spatiotemporal systems. Another important innovation of PIML is the Neural ODE framework introduced by Chen et al. (2018), which is designated to emulate the ODE dynamics end-to-end with a continuous depth. Liu et al. (2022) preserved the PDE form in a neural network by discretizing it on a finite difference grid and representing it by a convolutional neural network (CNN) with fixed weights. In the autoregressive stepping of the Neural ODE framework, preserving the mathematical form of the governing PDE, even partially, could mitigate the issue of error accumulation since it carries the underlying physics information. Wang et al. (2022) extended the Neural ODE framework with deterministic and stochastic encoders (NP-ODE) to build a physics-informed data-driven surrogate for FEA simulations with uncertainty quantification. Sholokhov et al. (2023) proposed a physics-informed Neural ODE (PINODE) model by adding an additional collocation reconstruction loss term to the ordinary loss function when building autoencoder-based reduced-order models (ROMs).

In terms of the application of PIML to the area of composites, Tao et al. (2021) employed the Neural ODE framework with a β-variational autoencoder (β-VAE) for feature extraction to learn the underlying dynamics of damage accumulation mechanism that describes the stiffness degradation of composite laminates by an ODE. Sharma et al. (2021) adopted PINNs to estimate the stresses in the tablets and interphase of a single-lap joint based on mechanics with pre-determined material properties. Akhare et al. (2023) developed a physics-integrated neural differentiable (PiNDiff) model where the system state is summed with a known, or partially known, PDE and showed its efficacy in an application to the curing process of composite prepregs.

However, these efforts did not include the end-to-end modeling of the whole manufacturing process. In the scope of a whole MMP with mechanical testing, the aforementioned efforts only handled parameters in certain single stages, not connecting the manufacturing process with the final quality measure. To the best of the authors' knowledge, the proposed PINOHI is the first work for end-to-end modeling of

the whole adhesive joint manufacturing process that bridges heterogeneous manufacturing parameters and the final quality measure.

3. The PINOHI Methodology

This section presents the development of PINOHI, which is a generalized Neural ODE framework with heterogeneous manufacturing controls and physical knowledge embeddings. Section 3.1 provides a brief introduction to basic Neural ODE. Section 3.2 introduces the formulations and details of the PINOHI model structure. Finally, section 3.3 describes the loss function for learning.

3.1 *Neural ODE Introduction*

Generally, Neural ODE (Chen et al., 2018) models a system of spatio-temporal ODEs/PDEs with a governing equation,

$$\frac{\partial \boldsymbol{u}(\boldsymbol{x},t)}{\partial t} = \mathcal{F}\left(\boldsymbol{u}, \nabla\boldsymbol{u}, \nabla^2\boldsymbol{u}, \dots; \boldsymbol{\lambda}_{phy}\right), \qquad \boldsymbol{x}, t \in \Omega_{s,t}, \tag{1}$$

and a boundary condition,

$$\mathcal{B}(\boldsymbol{u}, \nabla\boldsymbol{u}, \nabla^2\boldsymbol{u}, \dots) = 0, \qquad \boldsymbol{x}, t \in \partial\Omega_{s,t}, \tag{2}$$

where $\boldsymbol{u}(\boldsymbol{x},t) \in \mathbb{R}^n$ is the system state vector in the space and time coordinates $\boldsymbol{x}$, t, respectively, and $\nabla\boldsymbol{u}, \nabla^2\boldsymbol{u}, \dots$ are its spatial derivatives; $\boldsymbol{\lambda}_{phy}$ is the physical parameter vector/set; $\Omega_{s,t} = \Omega \times [0, T_s]$ is the spatial-temporal domain coupled by a physical domain Ω and a time span $[0, T_s]$, and $\partial\Omega_{s,t}$ is the corresponding boundary; $\mathcal{F}$ and $\mathcal{B}$ are the functions of dynamics and boundary conditions, respectively.

Neural ODE learns the system dynamics $\mathcal{F}$ using a neural network $f_{\boldsymbol{\theta}}$ with the system state and its spatial derivatives as input, which can be described as

$$\frac{\partial \boldsymbol{u}(\boldsymbol{x},t)}{\partial t} = f_{\boldsymbol{\theta}}(\boldsymbol{u}, \nabla\boldsymbol{u}, \nabla^2\boldsymbol{u}, \dots; \boldsymbol{x}, t), \qquad \boldsymbol{x}, t \in \Omega_{s,t}, \tag{3}$$

where f is a neural network with parameter $\boldsymbol{\theta}$.

3.2 *Model Structure of PINOHI*

There are two unique characteristics of the composite joint manufacturing process: (i) partially known process: as a multistage manufacturing process, the lap shear testing stage can be modeled as an ODE, while the effects of the manufacturing stages remain implicit; and (ii) additional control actions: manufacturing parameters control the physical process. Considering these two significant characteristics, we made a critical generalization of the Neural ODE model. To incorporate the partially known physical knowledge, we assume the following additive structure of the system dynamics function $\mathcal{F}$, i.e.,

$$\mathcal{F}(\cdot) = \mathcal{A}(\cdot) + \mathcal{R}(\cdot), \tag{4}$$

where $\mathcal{A}$ is the known physics from the analytical physics model and $\mathcal{R}$ is the residual to be learned. This assumption is based on the idea of residual modeling with $\mathcal{R}$ as the model discrepancy for "bias correction" to correct or mitigate the gap caused by a potentially mis-specified analytical physics model $\mathcal{A}$ due to partially known physics or oversimplified assumptions (Cross et al., 2022; Kennedy and O'Hagan, 2001).

Considering control variables in the manufacturing process, in addition to the physical parameters, we further incorporate the manufacturing parameters as the input for the residual part. Thus, the system becomes as follows:

$$\frac{\partial \boldsymbol{u}(\boldsymbol{x},t)}{\partial t} = \mathcal{A}\left(\boldsymbol{u}, \nabla\boldsymbol{u}, \nabla^2\boldsymbol{u}, \dots, \boldsymbol{\lambda}_{phy}\right) + \mathcal{R}\left(\boldsymbol{u}, \nabla\boldsymbol{u}, \nabla^2\boldsymbol{u}, \dots, \boldsymbol{\lambda}_{phy}, \boldsymbol{\lambda}_{mfg}\right), \qquad \boldsymbol{x}, t \in \Omega_{s,t}, \tag{5}$$

where the analytical physics part $\mathcal{A}$ needs calibration for unknown parameters, and the learnable residual part $\mathcal{R}$ can be further parameterized by a neural network $f_{\boldsymbol{\theta}_2}$ with parameter $\boldsymbol{\theta}_2$. Then, the model will become as

$$\begin{aligned}\frac{\partial \boldsymbol{u}(\boldsymbol{x},t)}{\partial t} = \varphi_{\boldsymbol{\theta}_1}\left(\mathcal{A}\left(\boldsymbol{u}, \nabla\boldsymbol{u}, \nabla^2\boldsymbol{u}, \dots, \hat{\boldsymbol{\lambda}}_{phy}, \boldsymbol{\lambda}^0_{phy}\right); \boldsymbol{x}, t, \boldsymbol{\lambda}_{mfg}\right) \\ + f_{\boldsymbol{\theta}_2}\left(\boldsymbol{u}, \nabla\boldsymbol{u}, \nabla^2\boldsymbol{u}, \dots; \boldsymbol{x}, t, \boldsymbol{\lambda}^0_{phy}, \boldsymbol{\lambda}_{mfg}\right), \boldsymbol{x}, t \in \Omega_{s,t},\end{aligned} \tag{6}$$

where $\varphi_{\boldsymbol{\theta}_1}$ is the calibration function learned by neural operators with parameter $\boldsymbol{\theta}_1$, the physical parameter vector/set $\boldsymbol{\lambda}_{phy} \coloneqq \left[\hat{\boldsymbol{\lambda}}_{phy}, \boldsymbol{\lambda}^0_{phy}\right]^T$ is divided into two parts: (i) $\hat{\boldsymbol{\lambda}}_{phy}$ is the calibrated value of the part in $\boldsymbol{\lambda}_{phy}$ that needs calibration, e.g., material properties, environment-related parameters, etc.; and (ii) $\boldsymbol{\lambda}^0_{phy}$ is the left part which is calibration-free, e.g., geometric dimensions, physical constants, etc. Specifically, in

addition to the physics of first-order dynamics learned by the Neural ODE structure, physics knowledge is incorporated from three parts: (i) the first part is the analytical approximation function $\mathcal{A}$ to the underlying unknown system dynamics $\mathcal{F}$; (ii) the second part comes from the manufacturing parameter vector/set $\boldsymbol{\lambda}_{mfg}$ in the calibration function $\varphi_{\boldsymbol{\theta}_1}$ of the analytical model; and (iii) the last part is the calibration-free physical parameter vector $\boldsymbol{\lambda}_{phy}^0$ and manufacturing parameter vector/set $\boldsymbol{\lambda}_{mfg}$ in both parts. The neural network $f_{\boldsymbol{\theta}_2}$ is designed to mitigate the gap between analytical function and the true dynamics. Note that the manufacturing parameter vector/set $\boldsymbol{\lambda}_{mfg}$ here refers to those parameters not included in the analytical function but still related to the system state of interest when modeling a complex manufacturing process. The physical parameter vector/set $\boldsymbol{\lambda}_{phy}$, in general, is some unknown function of $\boldsymbol{\lambda}_{mfg}$, and its estimated value $\hat{\boldsymbol{\lambda}}_{phy}$ is one of the inputs in analytical physics model $\mathcal{A}$.

As shown in Fig. 2, the proposed PINOHI structure follows the basic framework of Neural ODE that leverages system dynamics by outputting the first derivative for forward time-stepping and processes information in an autoregressive way. However, unlike conventional black-box methods, it also (i) incorporates physical knowledge by preserving the mathematical formula of the analytical physics model $\mathcal{A}$; and (ii) takes additional heterogeneous manufacturing parameters as control input of the Neural ODE network. The network structure is designed as follows:

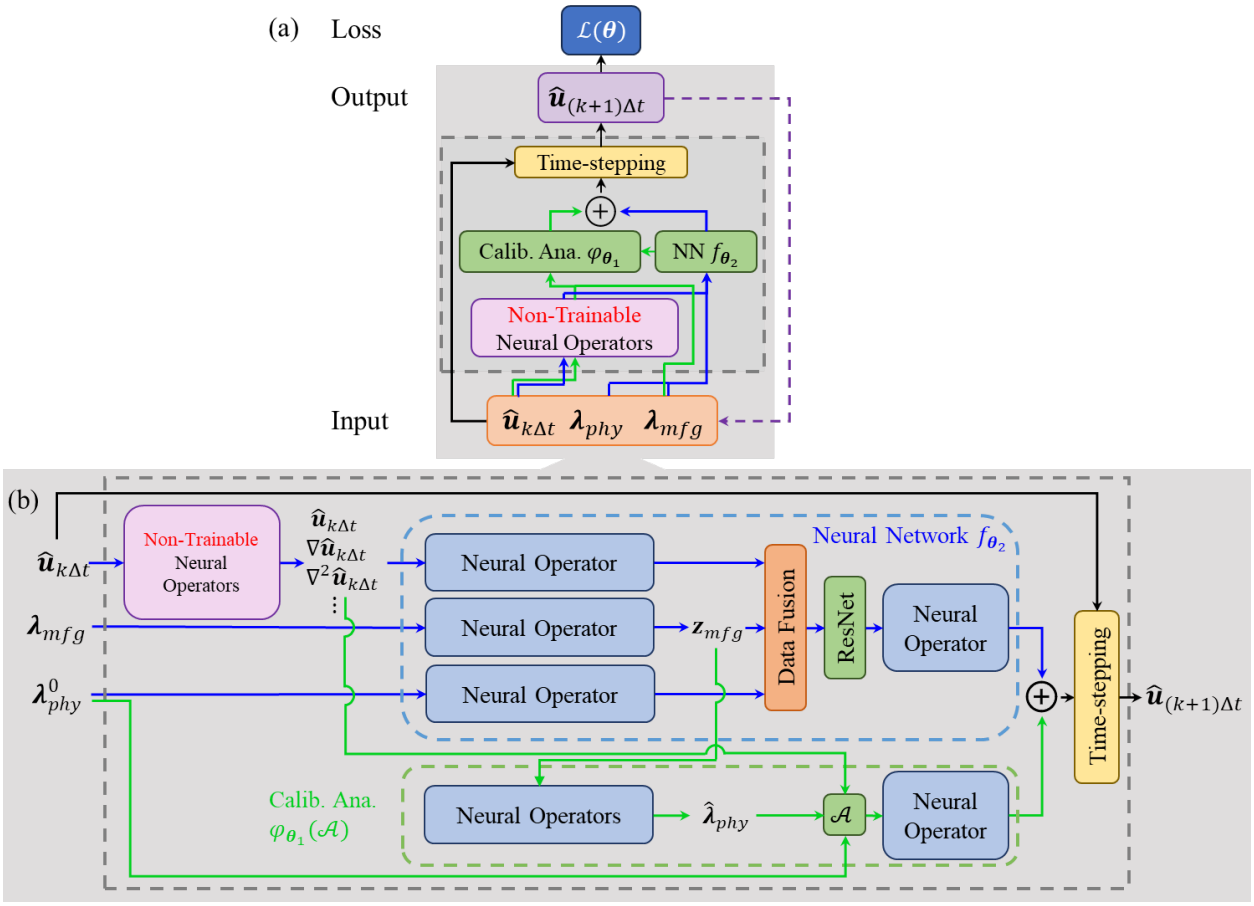

Fig. 2: (a) Overview of the PINOHI structure, where 'Calib. Ana.' and 'NN' denote the calibrated analytical physics function $\varphi_{\boldsymbol{\theta}_1}(\mathcal{A})$ and the neural network $f_{\boldsymbol{\theta}_2}$, and $\boldsymbol{\lambda}_{phy} = \left[\hat{\boldsymbol{\lambda}}_{phy}, \boldsymbol{\lambda}^0_{phy}\right]^T$. (b) Detailed structure of the iterative physics-informed unit in (a), which consists of $\varphi_{\boldsymbol{\theta}_1}(\mathcal{A})$ and $f_{\boldsymbol{\theta}_2}$ where neural operators represent linear or convolutional layers.

First, the predicted result from the last step, $\hat{\boldsymbol{u}}_{k\Delta t}$ is fed into non-trainable operators for computing the spatial derivatives of the system state $\hat{\boldsymbol{u}}_{k\Delta t}$ at time point $k\Delta t$, i.e., $\nabla\hat{\boldsymbol{u}}_{k\Delta t}, \nabla^2\hat{\boldsymbol{u}}_{k\Delta t}, \ldots$. This can be implemented by convolution operation using pre-defined kernels depending on the data structure of the system state. Then, to solve the heterogeneity issue, a data fusion layer is used to fuse the extracted features from the system state $\hat{\boldsymbol{u}}_{k\Delta t}$ with its spatial derivatives $\nabla\hat{\boldsymbol{u}}_{k\Delta t}, \nabla^2\hat{\boldsymbol{u}}_{k\Delta t}, \ldots$, the calibration-free physical parameter $\boldsymbol{\lambda}^0_{phy}$, and the heterogeneous manufacturing parameter vector/set $\boldsymbol{\lambda}_{mfg}$.

The neural operators marked in blue in Figure 2(b) and the embedded residual network (ResNet) are trainable. The selection of ResNet is because it can be regarded as a discretization of a continuous ODE, which is a natural choice in this scenario. The extracted manufacturing feature $\boldsymbol{z}_{mfg}$ and calibration-free physical parameter $\boldsymbol{\lambda}_{phy}^{0}$ are inputs for the calibration of the physical parameter $\hat{\boldsymbol{\lambda}}_{phy}$. The analytical approximation $\mathcal{A}$ then takes the calibrated $\hat{\boldsymbol{\lambda}}_{phy}$ together with calibration-free physical parameter $\boldsymbol{\lambda}_{phy}^{0}$ and system states $\hat{\boldsymbol{u}}_{k\Delta t}, \nabla\hat{\boldsymbol{u}}_{k\Delta t}, \nabla^2\hat{\boldsymbol{u}}_{k\Delta t}, \ldots$ as inputs. The embedded neural network is designed as stacked convolutional or linear residual network (He et al., 2016) blocks depending on the data format of the system state. Later, the results of the neural network $f_{\boldsymbol{\theta}_2}$ and the calibrated analytical physics model $\varphi_{\boldsymbol{\theta}_1}(\mathcal{A})$ are summed together as the first-order derivative of the system state, which is for a forward time-stepping, e.g., Euler or Runge-Kutta methods, with system state, to yield the next time step result $\hat{\boldsymbol{u}}_{(k+1)\Delta t}$.

3.3 *Loss Function*

The loss function $\mathcal{L}(\boldsymbol{\theta})$, similar as Wang et al. (2021), is defined as

$$\mathcal{L}(\boldsymbol{\theta}) = \frac{1}{T_s}\sum_{t=0}^{T_s}\left[\gamma_\beta \mathcal{L}_{MSE}(\boldsymbol{\theta}) + \left(1-\gamma_\beta\right)\mathcal{L}_{MSPE}(\boldsymbol{\theta})\right], \tag{7}$$

where

$$\mathcal{L}_{MSE}(\boldsymbol{\theta}) = \left\|\boldsymbol{u}_t - \hat{\boldsymbol{u}}_t\left(\boldsymbol{\lambda}_{phy}, \boldsymbol{\lambda}_{mfg}, \boldsymbol{\theta}\right)\right\|_2^2, \tag{8}$$

and

$$\mathcal{L}_{MSPE}(\boldsymbol{\theta}) = \sum_{\boldsymbol{x}\in\Omega}\sum_{i=1}^{n}\frac{\left[u_{\boldsymbol{x},t}^{i} - \hat{u}_{\boldsymbol{x},t}^{i}\left(\boldsymbol{\lambda}_{phy}, \boldsymbol{\lambda}_{mfg}, \boldsymbol{\theta}\right)\right]^2}{\left[u_{\boldsymbol{x},t}^{i}\right]^2}, \tag{9}$$

in which $\mathcal{L}_{MSE}(\boldsymbol{\theta})$ computes the mean squared error (MSE) between the prediction $\hat{\boldsymbol{u}}_t\left(\boldsymbol{\lambda}_{phy}, \boldsymbol{\lambda}_{mfg}, \boldsymbol{\theta}\right)$ using physical parameter vector/set $\boldsymbol{\lambda}_{phy}$, manufacturing parameter vector/set $\boldsymbol{\lambda}_{mfg}$, trainable parameter $\boldsymbol{\theta} = [\boldsymbol{\theta}_1, \boldsymbol{\theta}_2]^T$ and the label $\boldsymbol{u}_t$ at time point t; $\mathcal{L}_{MSPE}(\boldsymbol{\theta})$ measures the mean squared percentage error (MSPE). Specifically, $\hat{u}_{\boldsymbol{x},t}^{i}\left(\boldsymbol{\lambda}_{phy}, \boldsymbol{\lambda}_{mfg}, \boldsymbol{\theta}\right)$ is the i^{th} element in the predicted system state vector $\hat{\boldsymbol{u}}$ at spatial coordinate $\boldsymbol{x}$ and time point t using certain parameters $\left(\boldsymbol{\lambda}_{phy}, \boldsymbol{\lambda}_{mfg}, \boldsymbol{\theta}\right)$, and $u_{\boldsymbol{x},t}^{i}$ is its

corresponding label; $\|\cdot\|_2$ is the l_2 norm; $\gamma_\beta \in [0,1]$ is adjustable weight updated with the training epoch index β, which is a hyper-parameter balancing MSE and the MSPE. Generally, MSE can improve prediction on large values, while MSPE works well on small values. A suitable γ_β helps the loss robust to both large and small values and ensures an overall optimal functional curve prediction. Then the training process is implemented by solving the optimization problem as follows,

$$\boldsymbol{\theta}^* = \arg\min_{\boldsymbol{\theta}} \mathcal{L}(\boldsymbol{\theta}), \tag{10}$$

via gradient descent. Commonly used optimizers such as stochastic gradient descent (SGD) and Adam (Kingma and Ba, 2014) can be utilized. The implementation details are discussed in Section 4.3.

4. Quality Prediction of Composite Adhesive Joints

This section will present how to use the PINOHI model for bonding quality prediction of adhesively bonded composite joints. Section 4.1 will describe the analytical physics model for lap shear load dynamics. Section 4.2 will introduce the detailed trainable component of the PINOHI model. A comprehensive experimental study is conducted to validate the performance of the proposed method, including the leave-one-batch-out cross-validation in Section 4.3 and sensitivity analysis of training data samples size in Section 4.4.

4.1 *Analytical Physics Model for Lap Shear Load Dynamics*

The lap shear testing process of a quasi-static tensile load under displacement control with a fixed rate is modeled assuming the load as the system state and its evolution following an ODE,

$$\frac{\mathrm{d}F(\delta)}{\mathrm{d}\delta} = \mathcal{F}\big(F(\delta), \boldsymbol{\lambda}_{phy}\big) = \mathcal{F}\big(F(\delta), \boldsymbol{\lambda}_{mat}, \boldsymbol{\lambda}_{geo}\big), \tag{11}$$

where $F(\delta) \in \mathbb{R}$ is the load of a displacement-control lap shear process at displacement δ, the whole response is recognized as a functional curve but with various length, the physical parameter vector $\boldsymbol{\lambda}_{phy} = \big[\hat{\boldsymbol{\lambda}}_{phy}, \boldsymbol{\lambda}^0_{phy}\big]^T$ is categorized into material property vector $\hat{\boldsymbol{\lambda}}_{phy} \coloneqq \boldsymbol{\lambda}_{mat}$ and geometric dimension vector $\boldsymbol{\lambda}^0_{phy} \coloneqq \boldsymbol{\lambda}_{geo}$. The analytical physics model (Zimmermann et al., 2022) is as follows:

$$\mathcal{A}(F, \boldsymbol{\lambda}_{mat}, \boldsymbol{\lambda}_{geo}) = \frac{F^2}{2[2(U_1 + U_2) + U_a]}, \tag{12}$$

where

$$U_1 = \frac{b}{2E}\left[\frac{E^2 t^3}{12(1-\nu^2)^2}\int_0^l \left(w''(x)\right)^2 \mathrm{d}x + lt\left(\frac{F}{bt}\right)^2\right], \tag{13}$$

$$U_2 = \frac{F^2 c}{3Ebt}, \tag{14}$$

$$U_a = \frac{F^2 t_a}{4G_a bc}, \tag{15}$$

in which

$$\int_0^l \left(w''(x)\right)^2 \mathrm{d}x = \frac{\mu_1^3}{4}[2\mu_1 l(A_1^2 - B_1^2) + (A_1^2 + B_1^2)\sinh(2\mu_1 l) + 2A_1 B_1(\cosh(2\mu_1 l) - 1)], \tag{16}$$

$$A_1 = -\frac{t + t_a}{2} - \mu_1(l + c)B_1, \tag{17}$$

$$B_1 = -\frac{t + t_a}{2}\frac{\mu_2}{N}C_c + \frac{t + t_a}{2}\frac{1}{N}(\mu_2 C_l C_c + \mu_1 S_l S_c), \tag{18}$$

$$N = \mu_1 C_l S_c + \mu_2 S_l C_c - \mu_1(l + c)(\mu_2 C_l C_c + \mu_1 S_l S_c), \tag{19}$$

$$\mu_i = \sqrt{\frac{F}{D_i}} \text{ for } i = 1,2, \tag{20}$$

with $C_c = \cosh(\mu_2 c)$, $C_l = \cosh(\mu_1 l)$, $S_c = \sinh(\mu_2 c)$, $S_l = \sinh(\mu_1 l)$, $D_1 = Et^3 b/12(1-\nu^2)$, and $D_2 = 8D_1$.

In the analytical physics model $\mathcal{A}(F, \boldsymbol{\lambda}_{mat}, \boldsymbol{\lambda}_{geo})$, the material property vector $\boldsymbol{\lambda}_{mat} \coloneqq [E, \nu, G_a]^T$ involves elastic modulus of adherend E [MPa], Poisson's ratio of adherend ν [-], and shear modulus of adhesive G_a [MPa]; the geometric dimension vector $\boldsymbol{\lambda}_{geo} \coloneqq [b, c, t, l, t_a]^T$ contains joint width b [mm], half-length of bonded region c [mm], thickness of adherend t [mm], length of unbonded region l [mm], and thickness of adhesive t_a [mm]. Specifically, each of the material properties is considered as some unknown function of manufacturing parameter vector/set $\boldsymbol{\lambda}_{mfg}$. Note that these three material properties assume that both adhesive and adherend material are isotropic. In conclusion, the analytical physics model

provides an ideal value of the load dynamics in terms of displacement given a simplified assumption of isotropic material.

4.2 *Trainable Neural Operators and Embedded Residual Network in PINOHI*

The geometric dimension vector $\boldsymbol{\lambda}_{geo} = [b, c, t, l, t_a]^T$ here, as one of the inputs, is direct physical measurements of lap joint samples. The manufacturing parameter vector/set $\boldsymbol{\lambda}_{mfg}$ is divided into two parts: (i) manufacturing parameter vector/set for panel fabrication $\boldsymbol{\lambda}_{fab}$ (stage II in Figure 1); and (ii) manufacturing parameter vector/set for lap joining $\boldsymbol{\lambda}_{lap}$ (stage IV in Figure 1). Both two manufacturing parameters include controllable variables, process characterizations, and environmental factors involved in the manufacturing processes of composite adhesive lap joints. Namely, they are dwelling temperature distribution averaged over time during fabrication (superscript with F) and lap joining (superscript with J) cure process $\boldsymbol{T}^F_{avg}, \boldsymbol{T}^J_{avg} \in \mathbb{R}^{2\times 2}$ [°C], contact angle distribution on the bonding area of both adherends $\boldsymbol{\Psi}_A, \boldsymbol{\Psi}_B \in \mathbb{R}^{2\times 2}$ [°], total out-of-freezer time of adherend (superscript with C) and adhesive (superscript with A) t^C_{out}, t^A_{out} [s], minimum vacuum pressure during fabrication and lap joining cure process p^F_{min}, p^J_{min} [Pa], ramp-up rate and dwelling time of lap joining cure process r^J [°C/s] and t^J [s], flashes along bonding edges X_F [-], ambient temperature T^F_e, T^J_e [°C], and environment relative humidity H^T_e, H^J_e [%]. Among them, the nominal value of the curing parameters, i.e., ramp-up rate and dwelling time r^J, t^J, dwelling temperature T^F, T^J and vacuum pressure p^F, p^J, are controllable variables for the design of experiments, but some of the corresponding measurements $\boldsymbol{T}^F_{avg}, \boldsymbol{T}^J_{avg}, p^F_{min}, p^J_{min}$ are considered as process characterizations for model training and testing; contact angle distribution $\boldsymbol{\Psi}_A, \boldsymbol{\Psi}_B$ on the bonding area of each adherend is surface characterization; total out-of-freezer time of adherend and adhesive t^C_{out}, t^A_{out} are controllable variables; $T^F_e, T^J_e, H^F_e, H^J_e$ are environmental factors that are typically uncontrollable; and lastly, flashes along bonding edges X_F is a categorical variable representing the state of flashes, i.e., no flashes, flashes on one side, and flashes on both sides. Those parameters are summarized in Table 1.

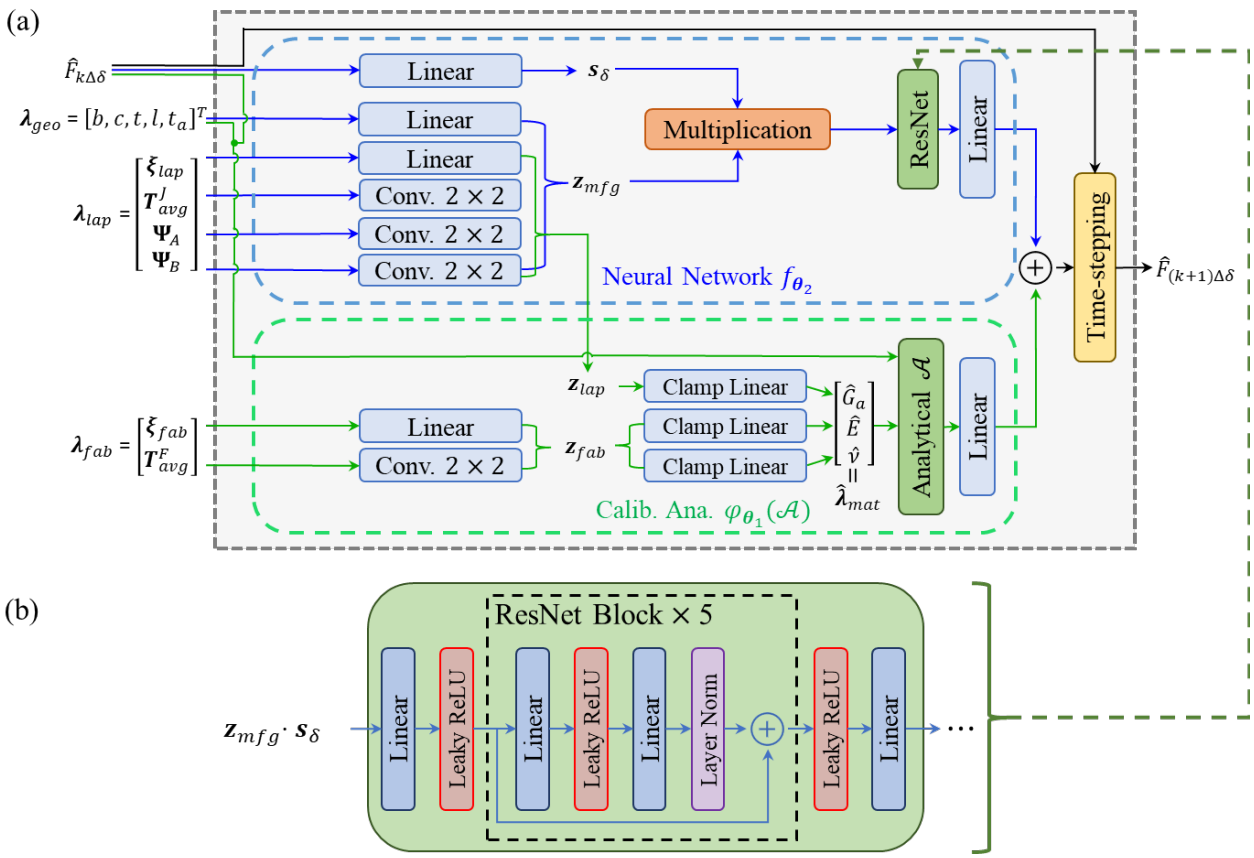

Fig. 3: (a) Detailed scheme of the iterative physics-informed unit for lap shear process. (b) Architecture of the embedded residual network.

As shown in Figure 3(a), the neural operators following the dwelling temperature distribution $\boldsymbol{T}^F_{avg}, \boldsymbol{T}^J_{avg}$ and contact angle distribution $\boldsymbol{\Psi}_A, \boldsymbol{\Psi}_B$ are defined as a convolutional layer with a 2×2 kernel. The geometric parameter vector $\boldsymbol{\lambda}_{geo} = [b, c, t, l, t_a]^T$ and sub-manufacturing vectors $\boldsymbol{\xi}_{fab} \coloneqq \left[t^C_{out}, p^F_{min}, T^F_e, H^F_e\right]^T$ and $\boldsymbol{\xi}_{lap} \coloneqq \left[t^A_{out}, r^J, t^J, p^J_{min}, T^J_e, H^J_e, X_F\right]^T$, composed of ramp-up rate and dwelling time r^J, t^J, total out-of-freezer time t^C_{out}, t^A_{out}, minimum vacuum pressure p^F_{min}, p^J_{min}, flashes X_F, environmental temperature and humidity $T^F_e, T^J_e, H^T_e, H^J_e$, are fed into a linear neural operator respectively. Both the convolutional channel and output size of linear layers are defined as a feature size of 16. Thus, the output of each feature extraction neural operator is a 16-dimensional vector, and they are stacked to form a feature matrix $\boldsymbol{z}_{mfg} \in \mathbb{R}^{5\times16}$. To be consistent with the structure of analytical function, the non-trainable

neural operator for taking derivatives of the load F is not included in the model for quality prediction of composite adhesive lap joint. The displacement δ is a scalar. A linear layer with output size of 16 is used to transform $\hat{F}_{k\Delta\delta}$ into a feature vector $\boldsymbol{s}_\delta \in \mathbb{R}^{16}$. Then the feature matrix $\boldsymbol{z}_{mfg}$ and the feature vector $\boldsymbol{s}_\delta$ are multiplied for data fusion as the input into the embedded residual network.

In the part of calibration for the analytical physics model, every entry of material property vector $\boldsymbol{\lambda}_{mat} = [E, \nu, G_a]^T$ is set as the output of a linear layer with output size of 1. The calibrated values of $\hat{E}, \hat{\nu}, \hat{G}_a$ will be the inputs for the analytical model together with current load $\hat{F}_{k\Delta\delta}$ and geometric dimension vector $\boldsymbol{\lambda}_{geo}$ of the analytical function. Specifically, (i) the Young's modulus E and Poisson ratio ν of adherend are determined by the manufacturing parameter vector/set in the curing process for panel fabrication ($\boldsymbol{\lambda}_{fab}$); and (ii) the shear modulus of adhesive G_a is determined by the manufacturing parameter vector/set in the curing process for lap joining ($\boldsymbol{\lambda}_{lap}$). This is because that the mechanical properties of adherend (E, ν) are only dependent on the panel fabrication stage and will not be influenced by the downstream joints curing. Note that the geometric dimension vector $\boldsymbol{\lambda}_{geo}$ is not used for calibration since they are not relevant to material properties. The output linear layer after the analytical model is a 1-to-1 transformation for scaling. This variable selection is engineering-domain-knowledge-driven which efficiently reduced the degree of freedom of the model, thus decreasing the required training samples to mitigate the issue of data scarcity.

The details of the embedded residual network are shown in Figure 3(b), where it is modeled as 5 stacked residual blocks. The output dimension is set the same as the input, which equals 5 since $\boldsymbol{z}_{mfg} \cdot \boldsymbol{s}_\delta \in \mathbb{R}^5$. The neural operator after this neural network is a 5-to-1 linear layer. All the hidden size in the residual blocks is $h = 128$. The activation functions of linear layers for the calibration of analytical function are softplus functions with a default parameter value of 1 to ensure positivity. These layers are further clamped within the range of 50% to 150% of their nominal values. All the remaining activation functions are leaky rectified linear units (Leaky ReLU) with negative slope of 0.01.

4.3 *Testing Experiments and Leave-One-Batch-Out Cross-Validation*

The testing experiments include a total of 15 batches of 77 lap joint samples that were made through the MMP described in Figure 1. Specifically, 11-ply CFRP panels were fabricated under the manufacturer's recommended cure cycle using an out-of-autoclave curing system. CFRP panels were then cut into $(l + 2c) \times b = 101.6$ [mm] $\times$ 25.4 [mm] pieces for surface treatment and characterization. The surface treatment is to apply artificial contamination on selected CFRP pieces. Lap joint samples were made of two CFRP pieces with $2c \times b = 25.4$ [mm] $\times$ 25.4 [mm] overlapping area that are bonded by an adhesive film after a secondary curing. These dimensions are per ASTM D5868-01. The adhesive film is with a nominal thickness of $t_a = 0.2413$ [mm]. The secondary curing is for joining. Lap shear testing was later conducted on the cured lap joint samples with a digital image correlation (DIC) system measuring the relative displacement. The load-displacement curves were exported afterwards.

In these 15 batches, the first 6 batches which contain 20 pristine and 6 contaminated samples are made per the manufacturer's recommended cure cycle of the secondary curing. The remaining 9 batches are manufactured according to the design of experiment result with 25 pristine and 26 contaminated samples in total. In detail, lap joining cure parameters r^J, t^J, p^J, T^J are considered as multilevel factors to formulate an orthogonal main-effect plan (Addelman, 1962). To keep a balanced dataset for the leave-one-batch-out cross-validation, from the set of manufacturer's recommended cure cycle, batch #6 is randomly selected. Thus, batch #6-15 were used in the leave-one-batch-out cross-validation.

The quality measure of composite adhesive lap joints is selected as the load-displacement curve $\boldsymbol{F}(\delta)$ for δ from 0 to the break value. Compared to a single value of the maximum load, the load-displacement curve contains more information, such as the overall stiffness of the adhesive joints at different strain levels and the total energy required to cause failure. The boundary condition of this specific case is

$$\mathcal{B}\big(F(\delta)\big) = F(0) = 0, \tag{21}$$

which is also an initial condition. This is intuitive since there will be no load exerted on the joints if it has no displacement.

In the training process, adjusting weight γ_β was set to 0.5 due to the similar magnitude of MSE and MSPE. The Adam optimizer was used with the initial learning rate of 0.001 and the coefficient of weight decay of 0.0001. A reduce-learning-rate-on-plateau scheduler was defined with a reducing factor of 0.5 and a waiting patience of 20. Also, 5 repetitions were carried out for each scenario and the average error with corresponding standard deviation are reported. The convergence is determined by an early stop criterion $\left|\mathcal{L}_\beta - \mathcal{L}_{\beta-1}\right|/\mathcal{L}_{\beta-1} \leq 0.001$ to avoid overfitting. All the training and testing processes were implemented by PyTorch in Python on NVIDIA GeForce RTX 3060 Laptop GPU. The average training and inference time are 2831.93 [s] and 0.50387 [s], respectively.

The mean absolute relative error (MARE) metrics (J. Chen et al., 2021) is selected as the error metric for each load-displacement curve since it computes the relative error in terms of the area under one curve, in this specific case of composite adhesive joints, naturally reflecting the total energy needed to break one joint, which is a mechanical characterization of the overall joint property, defined as,

$$MARE = \frac{\int \left|F(\delta) - \hat{F}(\delta)\right| \mathrm{d}\delta}{\int |F(\delta)| \, \mathrm{d}\delta}, \tag{22}$$

where $F(\delta)$ and $\hat{F}(\delta)$ are experimental and predicted loads at displacement level δ. Since MARE is designed for a single sample, the mean value over the testing set, i.e., mMARE, is computed and its average value over 5 repetitions is used for evaluation in each scenario in the cross-validation. The results of leave-one-batch-out cross-validation are compared among the following models, and summarized in Table 2, Figures 4:

1. **PINOHI**: The proposed model which combines analytical physics part $\varphi_{\boldsymbol{\theta}_1}(\mathcal{A})$ and neural network $f_{\boldsymbol{\theta}_2}$ with heterogeneous manufacturing parameter vector/set $\boldsymbol{\lambda}_{mfg}$ as control inputs.
2. **Neural ODE + Mfg.**: A generalization of Neural ODE $f_{\boldsymbol{\theta}_2}$ by incorporating heterogeneous manufacturing parameter vector/set $\boldsymbol{\lambda}_{mfg}$ as control inputs, which is equivalent to the proposed model PINOHI without the analytical physics part $\varphi_{\boldsymbol{\theta}_1}(\mathcal{A})$.

3. **Calib. Ana.**: Only the calibrated analytical physics model $\varphi_{\boldsymbol{\theta}_1}(\mathcal{A})$ using heterogeneous manufacturing parameter vector/set $\boldsymbol{\lambda}_{mfg}$ for calibration but without neural network $f_{\boldsymbol{\theta}_2}$ and feature extractor.
4. **Neural ODE**: Only the neural ODE structure $f_{\boldsymbol{\theta}_2}$ without: (i) the analytical physics function $\varphi_{\boldsymbol{\theta}_1}(\mathcal{A})$; and (ii) heterogeneous manufacturing parameter vector/set $\boldsymbol{\lambda}_{mfg}$.

Table 2: Results of leave-one-batch-out cross-validation of PINOHI vs. different ablated models.

mMARE (Average ± Std.) Over 5 Repetitions						
Models	**Scenario Index**					
	1	2	3	4	5	6
PINOHI	**0.2052 ± 0.0082**	**0.1131 ± 0.0051**	**0.1203 ± 0.0094**	**0.0772 ± 0.0188**	**0.0910 ± 0.0010**	**0.0724 ± 0.0050**
Neural ODE + Mfg.	0.2238 ± 0.0332	0.1289 ± 0.0100	0.1495 ± 0.0228	0.1151 ± 0.0192	0.0950 ± 0.0047	0.0986 ± 0.0130
Calib. Ana.	0.2765 ± 0.0006	0.1565 ± 0.0033	0.1688 ± 0.0012	0.1864 ± 0.0032	0.1010 ± 0.0001	0.0844 ± 0.0003
Neural ODE	0.2517 ± 0.0016	0.1269 ± 0.0075	0.1349 ± 0.0070	0.1581 ± 0.0186	0.0955 ± 0.0054	0.1056 ± 0.0057
Models	**Scenario Index**					
	7	8	9	10	Total Mean	
PINOHI	**0.0627 ± 0.0081**	**0.1069 ± 0.0110**	**0.0840 ± 0.0006**	**0.1091 ± 0.0127**	**0.1042 ± 0.0382**	
Neural ODE + Mfg.	0.0883 ± 0.0131	0.1654 ± 0.0184	0.1471 ± 0.0362	0.1660 ± 0.0189	0.1378 ± 0.0395	
Calib. Ana.	0.0687 ± 0.0004	0.1133 ± 0.0108	0.0910 ± 0.0009	0.1594 ± 0.0006	0.1406 ± 0.0592	
Neural ODE	0.0751 ± 0.0118	0.1433 ± 0.0081	0.0899 ± 0.0156	0.1468 ± 0.0014	0.1328 ± 0.0474	

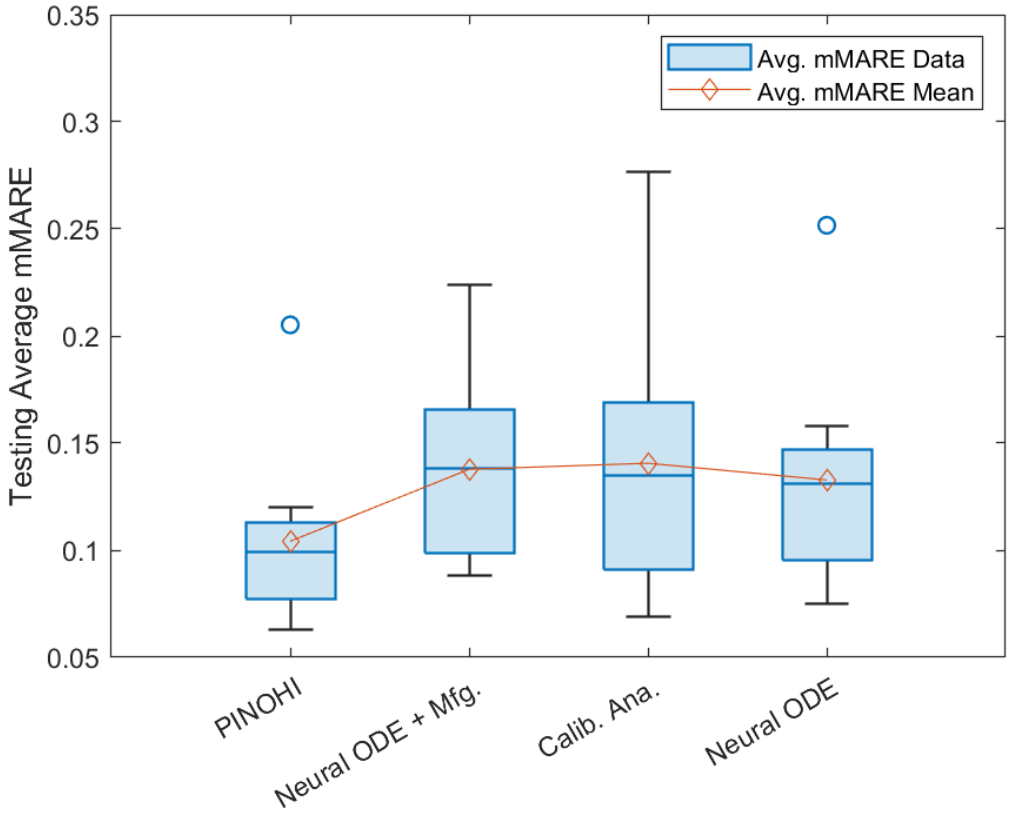

Fig. 4: Boxplots of average mMARE for all models in leave-one-batch-out cross-validation.

According to the results listed in Table 2, the proposed PINOHI model achieves the best average mMARE in each scenario of the leave-one-batch-out cross-validation. We provide a detailed analysis of the cross-validation study as follows:

1. As illustrated in Figure 4, in terms of the overall performance in the leave-one-batch-out cross-validation, PINOHI obtains the minimum total mean, median, and range of average mMARE, showing a superior performance over the other three ablated models.
2. The analytical model calibrated by heterogeneous manufacturing parameters (Calib. Ana.) is a common practice using physics-based models, which achieves the worst overall performance (Figure 4). This reflects the complexity of the system and the inadequacy of the simplified physical modeling assumptions.

3. On the other hand, PINOHI outperforms the data-driven methods (Neural ODE and Neural ODE + Mfg.), as shown in Figure 4, indicating that the inclusion of physics knowledge can significantly improve predictive accuracy in a complex system.

Overall, the proposed PINOHI method achieves the best performance which indicates that integration of heterogeneous manufacturing parameters and analytical physics equation can help the Neural ODE structure in greater prediction accuracy and a better generalization ability.

4.4 *Sensitivity Analysis of Samples in Training*

In addition to the leave-one-batch-out cross-validation, a sensitivity analysis of samples in training was performed to explore the minimum amount of data in training set required to achieve an adequately accurate prediction of the load-displacement curve in lap shear testing process. This is of great industrial interest and significance because the training data is time-consuming and expensive to collect due to its nature of the destructive testing methods.

In the sensitivity study, the testing set was randomly selected as batch #7 that contains 3 pristine and 2 contaminated samples. The remaining 72 samples formed the training set. In this sensitivity analysis, the amount of data in the training set starts from a small sample setting that only has 10 samples, and then increases with a step of 10 up to 60. The training samples were randomly sampled from the whole training set of 72 samples while keeping a balance between pristine and contaminated samples. For each case, 5 repetitions were conducted to mitigate the randomness of learning. Besides, this whole process was repeated 3 times to exploit the training space and to mitigate the randomness of selecting training sets. In other words, with batch #7 as the testing set, in total 3 rounds of sensitivity analysis of samples in training were carried out, in which 5 repetitions were run for each of the cases with the number of training samples varying from 10 to 72. The hyperparameters and error metric were set to be identical to those in the leave-one-batch-out cross-validation, and the average mMARE with its standard deviation over 3 rounds of 5 repetitions for each case is reported. The results of the sensitivity analysis are summarized in Table 3, Figures 5 and 6.

Table 3: Results of sensitivity analysis of PINOHI vs. different ablated models.

mMARE (Average ± Std.) Over 15 Repetitions (3 Rounds of 5 Repetitions)				
Models	**Samples in Training**			
	72	60	50	40
PINOHI	**0.1003 ± 0.0112**	**0.1087 ± 0.0060**	**0.1092 ± 0.0068**	**0.1078 ± 0.0065**
Neural ODE + Mfg.	0.1223 ± 0.0201	0.1137 ± 0.0089	0.1203 ± 0.0102	0.1268 ± 0.0247
Calib. Ana.	0.1147 ± 0.0017	0.1153 ± 0.0019	0.1146 ± 0.0035	0.1213 ± 0.0045
Neural ODE	0.1339 ± 0.0030	0.1370 ± 0.0037	0.1384 ± 0.0031	0.1387 ± 0.0035
Models	**Samples in Training**			
	30	20	10	
PINOHI	**0.1119 ± 0.0086**	**0.1115 ± 0.0124**	**0.1123 ± 0.0179**	
Neural ODE + Mfg.	0.1291 ± 0.0187	0.1344 ± 0.0253	0.1868 ± 0.0613	
Calib. Ana.	0.1265 ± 0.0122	0.1725 ± 0.0341	0.1780 ± 0.0116	
Neural ODE	0.1452 ± 0.0045	0.1394 ± 0.0038	0.1531 ± 0.0236	

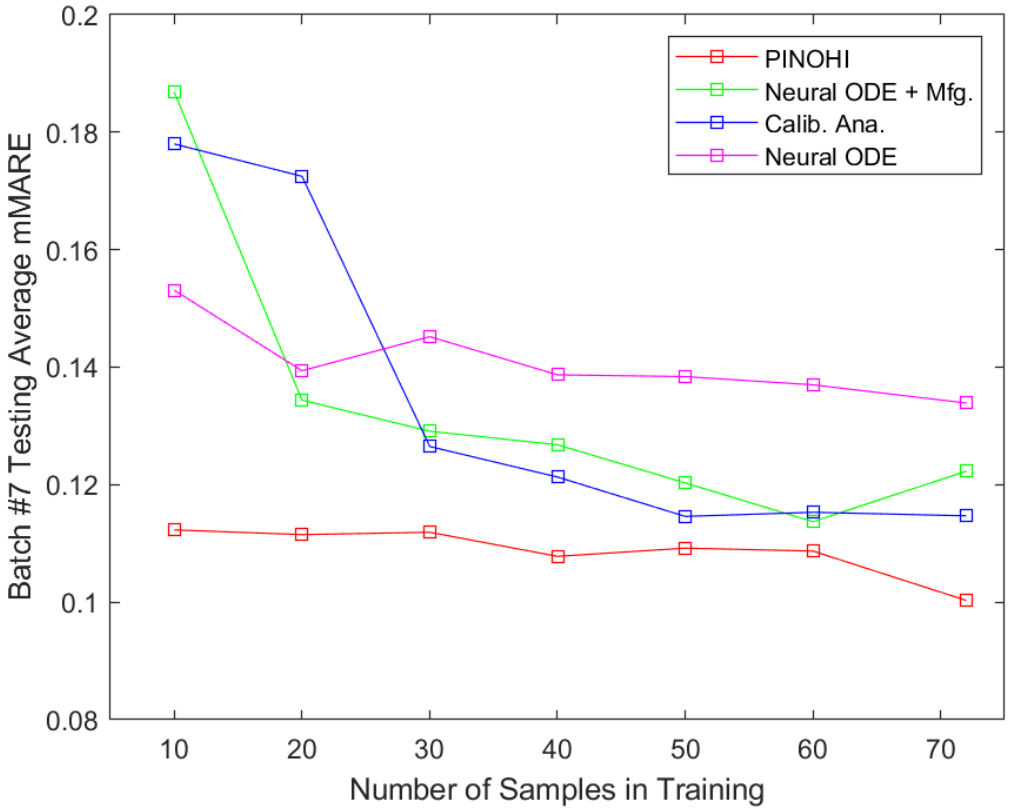

Fig. 5: Average mMARE of all models over different numbers of samples in training.

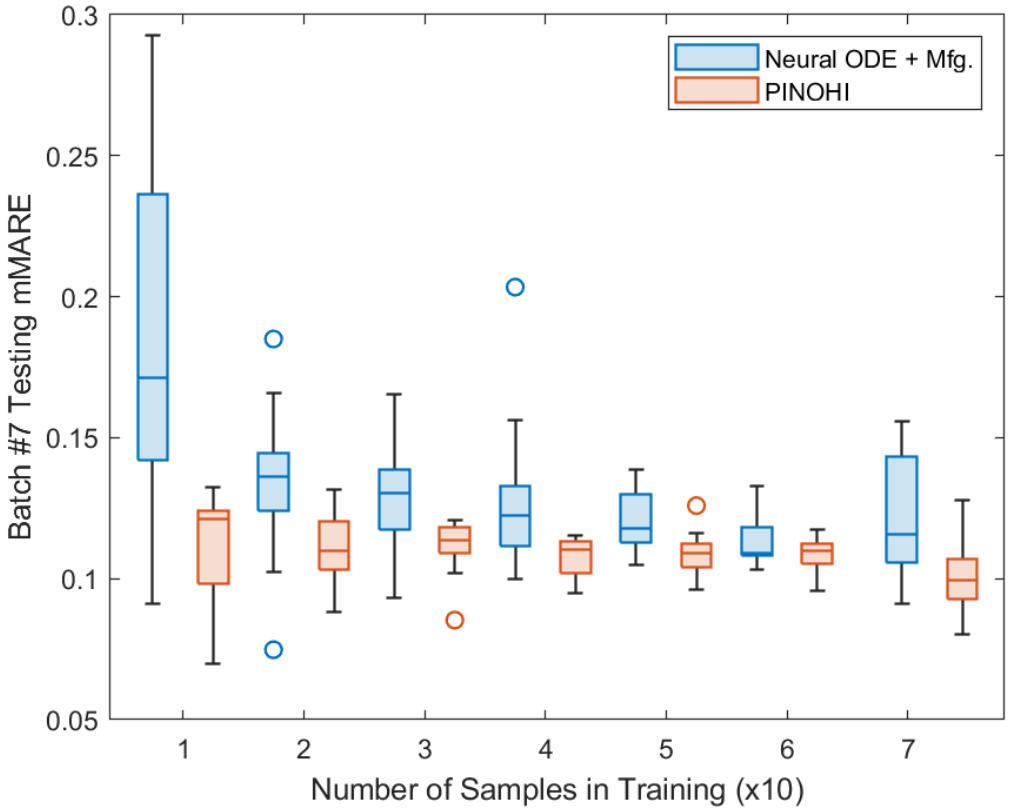

Fig. 6: Boxplots of mMARE for PINOHI vs. best competing model Neural ODE + Mfg. in the sensitivity analysis.

In each case in the sensitivity analysis, as shown in Table 3 and Figure 5, the average mMARE over 3 rounds of 5 repetitions achieved by PINOHI is consistently smaller than those of the competing models, maintaining a minimum variation across different training set sizes. Furthermore, a significant gap can be observed when the training set is small, i.e., equal to 10, which shows the advantage of PINOHI in the small sample scenario. This is because of the incorporation of analytical model into Neural ODE framework and the engineering-domain-knowledge-driven variable selection, which reduces the degree of freedom of the model. Moreover, the Calib. Ana. has a worse performance compared to PINOHI due to a lack of flexibility and over-simplified assumptions. In addition, the data-driven benchmark Neural ODE also remains a small variation with respect to the training set size, but it is significantly worse than PINOHI,

indicating the naïve Neural ODE structure cannot capture the complex dynamics without manufacturing parameters.

Besides the average performance, a more detailed comparison of the variability in different cases was explored by showing the boxplot of mMARE for PINOHI and the best competing model Neural ODE + Mfg. in Figure 6. Comparing with Neural ODE + Mfg., PINOHI has either smaller median mMARE or less variation or both in each case, indicating the analytical structure in PINOHI improves the robustness with respect to the number of samples in training.

In summary, PINOHI outperformed the other three competing modelling methods in each scenario of the sensitivity analysis and maintained a minimum variation, which demonstrates its superiority in predictive accuracy and robustness to the training set size.

5. Conclusion

Despite various efforts in the development of physics-based and data-driven models and methods for predicting the quality of composite adhesive joints, the complicated multi-stage manufacturing process hinders the accurate estimation of bonding quality. The bonding quality contains not only bonding strength, but also other important mechanical characterizations, e.g., stress-strain curves, overall bonding stiffness at different strain levels, total energy required to cause failure, etc.

In this study, a novel framework of physics-informed Neural ODE structure with heterogeneous manufacturing control inputs and physical knowledge embedding (PINOHI) is proposed for the quality prediction of composite adhesive joints. Compared with those models in the literature, PINOHI outputs the load-displacement curve in an autoregressive way from which the aforementioned mechanical characterizations can be derived easily. PINOHI incorporates additional physics knowledge and heterogeneous manufacturing parameters with an engineering domain knowledge-driven variable selection structure to mitigate the issue of data scarcity in the case of composite adhesive joints and improve predictive performance. Its superior performance on predicting load-displacement curves of the lap shearing

test is demonstrated in the leave-one-batch-out cross-validation compared to three ablated models, showing the benefits of adding the manufacturing controls and analytical function. A sensitivity analysis of samples in training is further explored to show the robustness of PINOHI with respect to the number of samples in training.

There are still rooms for improving the proposed PINOHI and its applications in to composite joining processes. First, an automatic stopping criterion can be added to the PINOHI framework rather than a user-defined stopping point to meet industrial demands in a one-stop fashion. Second, the current analytical model in PINOHI for the lap shearing process mainly focuses on the test stage, with an assumption that material is isotropic. Incorporating more advanced physics-based analytical or numerical models depicting the physics of different stages is expected to improve the predictive performance. Moreover, the data fusion method and embedded residual network in PINOHI can be substituted for different application cases. In conclusion, PINOHI provides a valid prototype of incorporating an analytical model into the neural ODE framework for the prediction of dynamics of complex physical processes, which has the potential for further extensions both methodologically and practically.

Acknowledgements

This material is based upon work supported by the National Science Foundation under Grant EEC-2052714. The authors acknowledge the generous support from NSF and member companies of the Composite and Hybrid Materials Interfacing (CHMI) IUCRC.

Data Availability

Due to the nature of the research, commercial supporting data is not available.

Notes on Contributors

Yifeng Wang received a BS degree in Mechanical Engineering from Huazhong University of Science and

Technology in 2021. He is currently pursuing a PhD degree with the H. Milton Stewart School of Industrial and Systems Engineering, Georgia Institute of Technology. His research interests include physics-informed machine learning and data analytics for process modeling of complex manufacturing systems. Mr. Wang is also a student member of the Institute of Industrial and Systems Engineers (IISE) and the Institute for Operations Research and the Management Sciences (INFORMS).

Shancong Mou got his PhD degree in Industrial Engineering, MS degree in Computational Science and Engineering from Georgia Institute of Technology, BS in Energy and Power Engineering from Xi'an Jiaotong University. Currently, He is an assistant professor in the Department of Industrial and Systems Engineering at the University of Minnesota, Twin Cities. His research focuses on AI/ML-enabled data analytics for quality and productivity improvement in complex engineering systems.

Jianjun Shi (https://sites.gatech.edu/jianjun-shi/) received BS and MS degrees in Automation from the Beijing Institute of Technology in 1984 and 1987, respectively, and a PhD degree in Mechanical Engineering from the University of Michigan in 1992. Currently, Dr. Shi is the Carolyn J. Stewart Chair and Professor at the Stewart School of Industrial and Systems Engineering, Georgia Institute of Technology. His research interests include the fusion of advanced statistical and domain knowledge to develop methodologies for modeling, monitoring, diagnosis, and control for complex manufacturing systems. Dr. Shi is a Fellow of four professional societies, including ASME, IISE, INFORMS, and SME, an elected member of the International Statistics Institute (ISI), a life member of ASA, an Academician of the International Academy for Quality (IAQ), and a member of National Academy of Engineers (NAE).

Chuck Zhang (https://sites.gatech.edu/chuck-zhang/) is an Eugene C. Gwaltney, Jr. Chair and Professor in the H. Milton Stewart School of Industrial and Systems Engineering at the Georgia Institute of Technology, Atlanta, GA, USA. He serves as the Director of the Center for Composite and Hybrid Materials Interfacing (CHMI), a National Science Foundation Industry/University Cooperative Research Center (IUCRC). He

received the BS and MS degrees in mechanical engineering from Nanjing University of Aeronautics and Astronautics, Nanjing, China, in 1984 and 1987, respectively, an MS degree in Industrial Engineering from the State University of New York at Buffalo in 1990, and the PhD degree in Industrial Engineering from the University of Iowa, Iowa City, IA, USA, in 1993. Dr. Zhang has authored over 220 refereed journal articles and 230 conference papers. He also holds 27 U.S. patents. Dr. Zhang is a fellow of Institute of Industrial & Systems Engineers (IISE). His current research interests include additive manufacturing (3D printing and printed electronics), advanced composite structures manufacturing and maintenance, bio-manufacturing, and applications of AI/ML to advanced manufacturing.

References

Addelman, S. (1962). Orthogonal main-effect plans for asymmetrical factorial experiments. *Technometrics*, **4**(1), 21-46.

Akhare, D., Luo, T., and Wang, J.-X. (2023). Physics-integrated neural differentiable (PiNDiff) model for composites manufacturing. *Computer Methods in Applied Mechanics and Engineering*, **406**, 115902.

Banea, M. D., and da Silva, L. F. (2009). Adhesively bonded joints in composite materials: An overview. *Proceedings of the Institution of Mechanical Engineers, Part L: Journal of Materials: Design and Applications*, **223**(1), 1-18.

Campilho, R. D., Banea, M. D., Neto, J., and da Silva, L. F. (2013). Modelling adhesive joints with cohesive zone models: Effect of the cohesive law shape of the adhesive layer. *International Journal of Adhesion and Adhesives*, **44**, 48-56.

Chen, J., Mak, S., Joseph, V. R., and Zhang, C. (2021). Function-on-function kriging, with applications to three-dimensional printing of aortic tissues. *Technometrics*, **63**(3), 384-395.

Chen, R. T., Rubanova, Y., Bettencourt, J., and Duvenaud, D. K. (2018). Neural ordinary differential equations. *Advances in Neural Information Processing Systems*, **31**.

Chen, Z., Liu, Y., and Sun, H. (2021). Physics-informed learning of governing equations from scarce data. *Nature Communications*, **12**(1), 6136.

Cross, E. J., Gibson, S. J., Jones, M. R., Pitchforth, D. J., Zhang, S., and Rogers, T. J. (2022). Physics-informed machine learning for structural health monitoring. *Structural Health Monitoring Based on Data Science Techniques*, 347-367.

Deb, A., Malvade, I., Biswas, P., and Schroeder, J. (2008). An experimental and analytical study of the mechanical behaviour of adhesively bonded joints for variable extension rates and temperatures. *International Journal of Adhesion and Adhesives*, **28**(1-2), 1-15.

Dugdale, D. S. (1960). Yielding of steel sheets containing slits. *Journal of the Mechanics and Physics of Solids*, **8**(2), 100-104.

Freed, Y., Salviato, M., and Zobeiry, N. (2022). Implementation of a probabilistic machine learning strategy for failure predictions of adhesively bonded joints using cohesive zone modeling. *International Journal of Adhesion and Adhesives*, **118**, 103226.

Gu, Z., Liu, Y., Hughes, D. J., Ye, J., and Hou, X. (2021). A parametric study of adhesive bonded joints with composite material using black-box and grey-box machine learning methods: Deep neuron networks and genetic programming. *Composites Part B: Engineering*, **217**, 108894.

He, K., Zhang, X., Ren, S., and Sun, J. (2016). Deep residual learning for image recognition, in *Proceedings of the IEEE Conference on Computer Vision and Pattern Recognition*, 770-778

Kang, H., Lee, J. H., Choe, Y., and Lee, S. G. (2021). Prediction of lap shear strength and impact peel strength of epoxy adhesive by machine learning approach. *Nanomaterials*, **11**(4), 872.

Karniadakis, G. E., Kevrekidis, I. G., Lu, L., Perdikaris, P., Wang, S., and Yang, L. (2021). Physics-informed machine learning. *Nature Reviews Physics*, **3**(6), 422-440.

Kennedy, M. C., and O'Hagan, A. (2001). Bayesian calibration of computer models. *Journal of the Royal Statistical Society: Series B (Statistical Methodology)*, **63**(3), 425-464.

Kingma, D. P., and Ba, J. (2014). Adam: A method for stochastic optimization. *arXiv preprint arXiv:1412.6980*.

Liu, X.-Y., Sun, H., Zhu, M., Lu, L., and Wang, J.-X. (2022). Predicting parametric spatiotemporal dynamics by multi-resolution PDE structure-preserved deep learning. *arXiv preprint arXiv:2205.03990*.

Nastos, C., and Zarouchas, D. (2022). Probabilistic failure analysis of quasi-isotropic CFRP structures utilizing the stochastic finite element and the Karhunen–Loève expansion methods. *Composites Part B: Engineering*, **235**, 109742.

Neto, J., Campilho, R. D., and Da Silva, L. (2012). Parametric study of adhesive joints with composites. *International Journal of Adhesion and Adhesives*, **37**, 96-101.

Owens, J. F., and Lee-Sullivan, P. (2000a). Stiffness behaviour due to fracture in adhesively bonded composite-to-aluminum joints I. Theoretical model. *International Journal of Adhesion and Adhesives*, **20**(1), 39-45.

Owens, J. F., and Lee-Sullivan, P. (2000b). Stiffness behaviour due to fracture in adhesively bonded composite-to-aluminum joints II. Experimental. *International Journal of Adhesion and Adhesives*, **20**(1), 47-58.

Pereira, A., Ferreira, J., Antunes, F., and Bártolo, P. (2010). Analysis of manufacturing parameters on the shear strength of aluminium adhesive single-lap joints. *Journal of Materials Processing Technology*, **210**(4), 610-617.

Raissi, M., Perdikaris, P., and Karniadakis, G. E. (2019). Physics-informed neural networks: A deep learning framework for solving forward and inverse problems involving nonlinear partial differential equations. *Journal of Computational Physics*, **378**, 686-707.

Rangaswamy, H., Sogalad, I., Basavarajappa, S., Acharya, S., and Manjunath Patel, G. (2020). Experimental analysis and prediction of strength of adhesive-bonded single-lap composite joints: Taguchi and artificial neural network approaches. *SN Applied Sciences*, **2**, 1-15.

Sharma, S., Awasthi, R., Sastry, Y. S., and Budarapu, P. R. (2021). Physics-informed neural networks for estimating stress transfer mechanics in single lap joints. *Journal of Zhejiang University-Science A*, **22**(8), 621-631.

Sholokhov, A., Liu, Y., Mansour, H., and Nabi, S. (2023). Physics-informed neural ODE (PINODE): Embedding physics into models using collocation points. *Scientific Reports*, **13**(1), 10166.

Sommer, D., Haufe, A., and Middendorf, P. (2022). A machine learning material model for structural adhesives in finite element analysis. *International Journal of Adhesion and Adhesives*, **117**, 103160.

Song, M.-G., Kweon, J.-H., Choi, J.-H., Byun, J.-H., Song, M.-H., Shin, S.-J., and Lee, T.-J. (2010). Effect of manufacturing methods on the shear strength of composite single-lap bonded joints. *Composite Structures*, **92**(9), 2194-2202.

Tao, C., Zhang, C., Ji, H., and Qiu, J. (2021). Application of neural network to model stiffness degradation for composite laminates under cyclic loadings. *Composites Science and Technology*, **203**, 108573.

Wang, S., Xu, Z., Stratford, T., Li, B., Zeng, Q., and Su, J. (2023). Machine learning approach for analysing and predicting the modulus response of the structural epoxy adhesive at elevated temperatures. *The Journal of Adhesion*, 1-19.

Wang, Y., Oyen, D., Guo, W., Mehta, A., Scott, C. B., Panda, N., Fernández-Godino, M. G., Srinivasan, G., and Yue, X. (2021). StressNet - Deep learning to predict stress with fracture propagation in brittle materials. *Npj Materials Degradation*, **5**(1), 6.

Wang, Y., Wang, K., Cai, W., and Yue, X. (2022). NP-ODE: Neural process aided ordinary differential equations for uncertainty quantification of finite element analysis. *IISE Transactions*, **54**(3), 211-226.

Zimmermann, J., Schalm, T., Sadeghi, M., Gabener, A., and Schröder, K.-U. (2022). Analytical stiffness analysis of adhesively bonded single-lap joints subjected to out-of-plane deflection due to tensile loading. *The Journal of Adhesion*, **98**(11), 1635-1662.